PAPER
Ming Li, J. Ruud van Ommen *et al.*
The effects of SO_2 impurities on CO_2 electroreduction on bare silver and SiO_2 coated silver in different cell geometries

PAPER

Check for updates

The effects of SO$_2$ impurities on CO$_2$ electroreduction on bare silver and SiO$_2$ coated silver in different cell geometries†

Ming Li, [iD] *[a] Shilong Fu,[b] Ruud Kortlever [iD] [b] and J. Ruud van Ommen [iD] *[a]

Electrochemical CO$_2$ reduction presents an opportunity to transform waste flue gas with water and renewable electricity into chemicals or fuels. However, the energy-intensive nature of purification of flue gas underscores the appeal of directly utilizing the flue gas streams containing impurities. In this study, we investigate the impact of SO$_2$ impurities on CO$_2$ electroreduction in two electrochemical cell geometries: an H-cell and a membrane electrode assembly (MEA) cell. We observe distinctly different behavior of the Ag on carbon black (Ag/CB) catalyst under SO$_2$ impurities in the H-cell compared to the MEA cell, where SO$_2$ impurities exhibit a more pronounced effect on Ag/CB catalysts in the H-cell than in the MEA cell. This difference is attributed to the higher solubility of SO$_2$ in the electrolyte compared to CO$_2$, resulting in an accumulation effect and causing differences in the SO$_2$ concentration near the electrode between the H-cell and the MEA system. By depositing a very thin SiO$_2$ coating on the outermost surface of the Ag/CB catalyst using atomic layer deposition (ALD), the impact of SO$_2$ on the catalyst's selectivity is diminished. This is attributed to the permeability difference between CO$_2$ and SO$_2$ through the SiO$_2$ coatings and results in a local SO$_2$ concentration difference between samples with and without SiO$_2$ coatings.

Introduction

With the ongoing rise in global CO$_2$ emissions, there is an urgent need to develop sustainable technologies for capturing and utilizing CO$_2$. The electrochemical reduction of CO$_2$ offers an appealing method for transforming surplus CO$_2$, along with water and renewable electricity, into bulk chemicals that can be directly used in the process industry or as fuels, as depicted in Fig. 1. The electrochemical reduction of CO$_2$ to CO is particularly intriguing as this is a two-electron reduction product, resulting in significant yields from each mole of electron transfer.[1] Silver (Ag) is one of the best catalysts for the electroreduction of CO$_2$ to CO because of its high selectivity for CO during CO$_2$ reduction and its high stability over prolonged periods of operation.[2–5] However, the Ag catalyst is susceptible to poisoning and subsequent loss of activity during the reaction due to the presence of impurities in the reactants.[6–9] And the CO$_2$ streams from industry often contain a variety of pollutants,

and the CO$_2$ concentration typically is relatively low, compared to the close to 100% for carbon capture from the air or from seawater (ranging from 3 to 45% from power plants and steel manufacturing factories).[10] The anticipated costs of capturing CO$_2$ from a biomass-fueled combustion power plant range from \$150 to \$400 per metric ton of CO$_2$.[11] Furthermore, purification expenses for this procedure are projected to be between \$70 and \$275 per metric ton of CO$_2$.[11] Despite the implementation of costly purification procedures, trace amounts of contaminants persist in the gas feed.[12,13] Contaminants can pose a significant challenge to the long-term operation of Ag catalysts in industrial applications. Hence, it is crucial to study the CO$_2$ reduction reaction (CO$_2$RR) on Ag catalysts in the presence of varying concentrations of impurities. Furthermore, it is also important to develop strategies for protecting the catalysts from exposure to impurities and alleviating the poisoning issue.

Unprocessed flue gas emissions contain various gaseous impurities, the concentration of each impurity significantly depends on the emission source and, hence, the type of industry. Typically, flue gas emitted from power plants contains impurities such as sulfur oxides (SO$_x$), nitrogen oxides (NO$_x$), oxygen, and volatile organic compounds (VOC).[14,15] Hee Ko *et al.* have studied the impact of nitrogen oxides on electrochemical CO$_2$RR.[16] They used various NO$_x$ (including NO, NO$_2$, and N$_2$O) on Cu, Ag, and Sn catalysts in a flow cell and found that the presence of NO$_x$ (up to

[a] Department of Chemical Engineering, Faculty of Applied Sciences, Delft University of Technology, Van der Maasweg 9, 2629 HZ Delft, The Netherlands.
E-mail: M.Li-5@tudelft.nl, J.R.vanOmmen@tudelft.nl
[b] Process & Energy Department, Faculty of Mechanical Engineering, Delft University of Technology, Leeghwaterstraat 39, 2628 CB Delft, The Netherlands
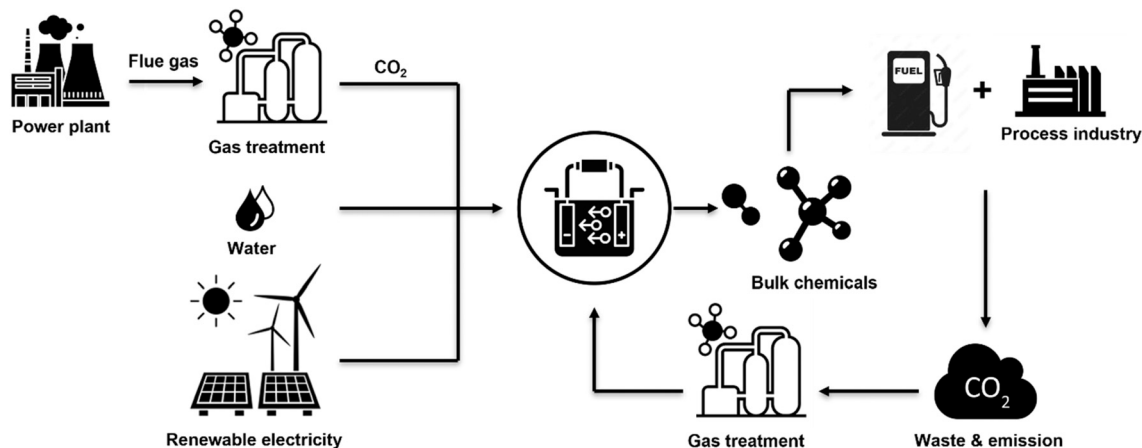† Electronic supplementary information (ESI) available. See DOI: https://doi.org/10.1039/d4cy01196a

2148 | *Catal. Sci. Technol.*, 2025, **15**, 2148–2159

This journal is © The Royal Society of Chemistry 2025

Fig. 1 Schematic illustration of the concept for CO_2 electroreduction in industry.

0.83 vol%) in the CO_2 feed results in a notable reduction in Faradaic efficiency (FE) during CO_2 electroreduction. This reduction is attributed to the preferential electroreduction of NO_x over CO_2. However, despite the decrease in FE, when the pure CO_2 feed is restored, the electrocatalyst maintains similar CO_2 reduction capabilities. This indicates that the enduring impact of NO_x on the catalytic performance of the modeled catalysts is negligible over the long term. Xu *et al.* found that when O_2 impurities are present at typical concentrations (4 vol% of O_2), most of the current was redirected from CO_2RR towards the oxygen reduction reaction (ORR).[17] This poses more serious issues when operating at elevated pressures. For example, 99% of the current was redirected to ORR at 15 bar. Van Daele *et al.* studied the stability of Ag and Bi_2O_3 catalysts with 198 ppm SO_2 in CO_2 and 213 ppm NO in CO_2 over the course of 20 h.[18] They found that the studied catalysts have a stable performance and high Faradaic efficiencies towards the target products over 20 h. Therefore, it seems that operating with 200 ppm of NO and SO_2 in the gas feed will not have much effect on the catalyst during CO_2RR. However, the presence of oxygen will significantly suppress the FE towards target products during CO_2RR; with 1 vol% of O_2 added to the stream, 23% of the FE towards CO_2RR was lost. This likely is due to the fact that the oxygen impurity has a higher concentration than NO and SO_2, and the preferential reduction of O_2 compared to CO_2 during the reaction. Albertini *et al.* found that using a passivation layer such as metallic oxides coatings can preserve catalyst's activity and improve its stability for CO_2 reduction.[19] Based on the aforementioned reports, we may infer that the impurities primarily affect the CO_2RR through competing reactions, rather than the poisoning effects that will lead to a long-term influence on the catalysts. Moreover, these studies are all carried out in flow cell reactors, while an H-cell system may give additional insights, as it can provide additional perspectives into the intrinsic properties of the catalyst by decoupling some of the complexities introduced in flow cells.

The objective of this paper is to determine the effect of SO_2 impurities on the Ag catalyst for the electrochemical reduction of CO_2 in two different cell geometries: an H-cell and a membrane electrode assembly (MEA) cell. We select SO_2 as the impurity for this study since it is found in most flue gases and sulfur has a pronounced poisoning effect on Ag catalysts.[7–9] We find that SO_2 has a more pronounced impact on Ag on carbon black (Ag/CB) catalysts in the H-cell compared to in the MEA reactor. This is attributed to the higher solubility of SO_2 in the electrolyte compared to CO_2, leading to an accumulation effect in the H-cell. This causes a higher SO_2 concentration near the electrode surface in the H-cell system than in the MEA reactor system. We use thermal atomic layer deposition (ALD) to deposit SiO_2 on Ag/CB catalyst to protect it from SO_2 impurities. ALD is a gas phase coating technique based on the alternating use of two reactants, depositing a thin film on a substrate. It provides sub-nanometer precision in coating thickness, controlled by the number of deposition cycles.[20] After applying 2 to 8 cycles of SiO_2 ALD providing a nanocoating on the outer surface of the Ag/CB catalyst, the effect of SO_2 on the selectivity of the catalyst is diminished at less negative potentials. This is attributed to the permeability difference between CO_2 and SO_2 through SiO_2 coatings.

Experimental

Materials

Silicon tetrachloride ($SiCl_4$, 99%) and iridium oxide (IrO_2) were purchased from Alfa Aesar, isopropanol (≥98%) was purchased from Honeywell, Nafion™ perfluorinated resin solution (5 wt% in lower aliphatic alcohols and 15–20% water) was purchased from Sigma-Aldrich. Deionized water with a resistivity of 18 MΩ cm was used as the co-reactant for ALD. 20 wt% of Ag on Carbon black-Vulcan XC 72R catalyst, Carbon Black Vulcan XC 72R, and Sigracet 39BB carbon paper gas diffusion layers (GDL) pretreated with PTFE in microporous layer were purchased from FuelCell store. Glassy carbon plates were ordered from HTW Hochtemperatur-

This journal is © The Royal Society of Chemistry 2025

Catal. Sci. Technol., 2025, **15**, 2148–2159 | **2149**

Werkstoffe GmbH (Germany). The electrolyte solution was prepared from ultrapure water (Milli-Q IQ 7000, 18.2 MΩ cm). PiperION® anion exchange membrane, 20 microns, was purchased from FuelCell store and submerged in the electrolyte overnight prior to MEA experiments. Potassium bicarbonate (KHCO$_3$, 99.95%) was purchased from Sigma-Aldrich. Anion exchange membrane (Selemion AMV) was purchased from AGC Engineering and kept in deionized water after receiving, and used for H-cell experiments. Ag nanopowder with a particle size from 20–40 nm and without oxide layer was purchased from Thermo Fisher Scientific. All chemicals were received and used without further purification.

Electrode preparation

Electrodes used in H-cell experiments. The Ag/CB catalyst was first drop casted on the glassy carbon electrode before the ALD coating. The catalyst ink was prepared by combining 4 mg of catalyst with 800 μL of deionized water, 180 μL of isopropanol, and 20 μL of Nafion perfluorinated resin solution in a vial. The mixture was then sonicated in an ice bath for 1 hour. Following this, 25 μL of the catalyst ink was drop-cast onto the surface of the glassy carbon electrode each time and this process was repeated four times to achieve a homogeneous deposition on the electrode. The SiO$_2$ coatings on the catalyst were then deposited in a custom-built flat substrate ALD reactor[20–22] operating at atmospheric pressure. The reactor chamber comprises a metal cylinder with an inner diameter of 40 mm and a length of 190 mm, accompanied by a substrate holder with dimensions of 30 mm by 125 mm. To ensure a uniform temperature profile, the deposition temperature was monitored and regulated using two thermocouples positioned inside and outside the ALD reactor. We opted for atmospheric pressure ALD over vacuum ALD as it reduces investment costs and enhances throughput at a larger scale.[21,22] Our SiO$_2$ deposition process was adapted from literature,[23] but the reaction time and precursor gas flow rate were adjusted based on our own requirements and still under the saturation conditions.[24] In summary, the SiCl$_4$ and H$_2$O, the ALD reactants, were filled in stainless steel bubblers and kept at room temperature. Nitrogen gas, with a purity of 99.999%, served as both carrier and purging gas, flowing at a rate of 0.5 L min^{-1} throughout the process, parallel to the substrate surface in the reactor. Before each experiment, samples underwent air plasma pre-treatment at room temperature and 4 mbar pressure for 60 seconds using a Harrick plasma machine. The ALD reactor was heated to and maintained at 100 °C throughout the process. SiCl$_4$ was introduced into the reactor for 15 second pulses, followed by 60 second purging with N$_2$ and 30 second dosing of H$_2$O vapor. A final 60 second purging with N$_2$ completed one ALD cycle. Detailed SiO$_2$ ALD operation conditions are available in Table S1.† Samples with varying numbers of ALD cycles were obtained by repeating the ALD cycles as needed. Upon completion of the synthesis process,

the reactor was purged with N$_2$ flow for 15 minutes and cooled to room temperature.

Electrodes used in MEA experiments. The catalyst used during the MEA experiments was synthesized using a vibrated fluidized bed reactor[25–27] operating at atmospheric pressure. A vibrating table was used at a frequency of 60 Hz to fluidize the powders and create uniform fluidization inside the reactor during the reaction. A glass column with an inner diameter of 2.5 cm was used as the reactor. 0.5 g of Ag/CB catalyst (pre-dried at 80 °C for 3 hours before the experiment, to remove the moisture) was used for each synthesis batch in the reactor. The SiCl$_4$ and H$_2$O, the ALD reactants, were filled in stainless steel bubblers and kept at room temperature. Nitrogen gas, with a purity of 99.999%, served as both carrier and purging gas throughout the reaction. A compensation N$_2$ stream with a flow rate of 1.5 L min^{-1} was employed during the SiCl$_4$ dosing period to maintain an equal gas flow of 2 L min^{-1} throughout the whole ALD process and keep the fluidization of the powders inside the reactor. The ALD reactor was heated to and maintained at 100 °C throughout the process. SiCl$_4$ was introduced into the reactor for 60 second pulses, followed by 150 second purging with N$_2$ and 60 second dosing of H$_2$O vapor. A final 150 second purging with N$_2$ completed one ALD cycle. By repeating the same ALD cycles for 4 times, 4 cycles coated sample was achieved. After the synthesis procedure, the fluidized bed reactor was purged for 15 minutes with N$_2$ flow to remove the residual reactants. Detailed SiO$_2$ ALD operation conditions were shown in Table S1.† The 4 cycles SiO$_2$ coated Ag/CB powders synthesized using the aforementioned method was utilized to prepare the ink that can be airbrushed on the GDL for the MEA experiments. The ink formula is very similar to the previously mentioned ink formula used for the H-cell experiments. In general, 4 mg of catalyst with 800 μL of isopropanol, 180 μL of deionized water, and 20 μL of Nafion perfluorinated resin solution were mixed in a vial. The mixture was then sonicated in an ice bath for 1 hour. After that, the ink solution was airbrushed onto the GDL using an airbrush gun and N$_2$ flow to reach a catalyst loading of 0.2 mg cm^{-1}.

Gas mixing steps for SO$_2$ impurities experiments. A gas mixing apparatus (Environics® Series 4000) was employed to mix the feed gas and ensure precise control over gas proportions for the electrochemical tests. To protect against the potential corrosion induced by SO$_2$, a precautionary measure was taken by coating the mass flow controllers and gas tubing within the testing system with SilcoNert® and sealing them with Kalrez®. The generation of varied concentrations of SO$_2$ gas was achieved by using two standard gas cylinders containing SO$_2$ with concentrations of 100 ppm and 10 000 ppm, balanced with CO$_2$ from Linde Gas. The pure CO$_2$ gas used in the experiments was also from Linde Gas with a purity of 99.999%. Detailed information regarding the gas recipes used for the electrochemical tests can be found in Table S2.†

Material characterization. X-ray photoelectron spectroscopy (XPS) analyses were conducted utilizing the Thermo Scientific™

2150 | *Catal. Sci. Technol.*, 2025, **15**, 2148–2159

This journal is © The Royal Society of Chemistry 2025

K-alpha™ instrument from ThermoFisher™ Scientific. The instrument employed monochromatic X-ray beams of aluminum Kα radiation (1486.7 eV) with a spot size of 400 μm. For the survey scans, a pass energy of 200 eV and a step size of 1 eV were employed, while higher-resolution spectra were obtained using a pass energy of 50 eV and a step size of 0.1 eV. All peak positions were analyzed and calibrated with reference to the aliphatic C 1s peak at 284.8 eV, utilizing CasaXPS software.

XPS area scan was performed with a Thermo Scientific™ K-alpha™ (ThermoFisher™ Scientific) utilizing a monochromatic X-ray of aluminum Kα radiation (1486.7 eV) and a circular area was chosen with a diameter of 12 mm. 121 points were selected and evenly distributed within the circular area. A pass energy of 153 eV and a dwell time of 0.5 s were used. The data was analyzed and plotted using the Avantage software.

Electrochemical measurements

Electrochemical measurements in H-cell. The electrochemical measurements were conducted using a H-cell setup.[28] A leak-free Ag/AgCl reference electrode (sat. KCl) was employed, alongside a counter electrode consisting of IrO_2-coated glassy carbon electrode. All potentials employed in this study were adjusted to the RHE scale using the following equation:[29]

$$E_{RHE} = E_{Ag/AgCl} + 0.197 + 0.059 \times pH$$

A 0.1 M solution of $KHCO_3$ served as the electrolyte in both chambers, and each chamber contains 1.8 mL of electrolyte. An anion-exchange membrane, Selemion AMV, was utilized to separate the anode and cathode chambers of the H-cell. Electrochemical measurements were conducted using a Biologic SP-200 potentiostat. Potentiostatic electrochemical impedance spectroscopy was utilized to evaluate the ohmic loss of the cell and was compensated for each experiment. Chronoamperometric measurements were carried out at different applied potentials from −0.8 to −1.2 V vs. RHE and were used to determine the FE of the catalysts. Before each experiment, the cathode electrolyte was purged with feeding gas for 15 minutes. The gas products were analyzed by an in-line gas chromatography (GC) (Compact GC4.0, Global Analyzer Solutions). Every 2 minutes the products were analyzed by the GC for quantification. The gas flow rate used during the experiments was kept at 8 sccm for every tests.

Electrochemical measurements in MEA. The electrochemical measurements were conducted using a MEA reactor purchased from Dioxide Materials. It is a 5 cm² CO_2 MEA electrolyzer cell coupled with a stainless steel flowfield plate with a serpentine channel in contact with the cathode GDE and a titanium flowfield plate with a serpentine channel in contact with the anode GDE. The reactor was assembled with 2 N*m Torque to ensure a leak-free assembly. The working electrode was prepared using the aforementioned method. The counter electrode was an IrO_2 airbrushed GDE.

The anion-exchange membrane used in the MEA was a PiperION® anion exchange membrane. 40 ml of 1 M $KHCO_3$ solution was used and circulated with a flow rate of 5 ml min⁻¹ in the anode serpentine channel. Use of 0.1 M $KHCO_3$ electrolyte in H-cell configurations and 1 M $KHCO_3$ electrolyte in MEA configurations are widely reported in the literature and facilitates comparisons across different studies. Employing 0.1 M $KHCO_3$ electrolyte in the MEA configuration can result in a very high Faradaic efficiency toward H_2 and a significantly low FE toward CO, thereby diminishing its relevance for CO_2 reduction studies. Chronopotentiometry measurements were carried out at different current densities and were used to determine the FE of the catalysts. The current density was calculated by dividing the applied current by the geometric area of the working electrode. CV measurements were carried out from 0.2 V to −1.0 V at a scan rate of 10 mV s⁻¹. The gas products were analyzed using the same in-line GC as described in the H-cell experiments; the gas flow rate used during the experiments was 20 sccm for every test.

Results and discussion

SO₂ impurities effects on CO₂ electroreduction in H-cell reactor

We first examined the effect of SO_2 impurities on the Ag/CB catalyst for CO_2 electroreduction in the H-cell system. A series of Ag/CB samples coated with SiO_2 were synthesized using ALD with a flat substrate reactor and compared with an uncoated Ag/CB sample. As demonstrated in our previous study,[30] thick SiO_2 coatings can reduce the catalyst activity. Therefore, in this study, we limited the deposition to a maximum of 8 cycles to avoid compromising catalyst performance. Based on the reported growth per cycle of SiO_2 using $SiCl_4$ under the experimental conditions, which is approximately 2 Å per cycle,[31,32] a very thin SiO_2 layer ranging from 0.4 nm to 1.6 nm is anticipated after 2 to 8 cycles of ALD coating. To determine the actual Ag weight percentage in the original Ag/CB nanoparticles, the sample underwent characterization through thermogravimetry differential thermal analysis (TG/DTA). The TG/DTA analysis (Fig. S1†) showed that roughly 22 wt% of Ag_2O residues were present after the analysis and revealed approximately 20 wt% of Ag in the original Ag/CB samples, and this number matches the metal loading specified in the documentation from the supplier. The rate of SiO_2 deposition was characterized via X-ray photoelectron spectroscopy (XPS), with Fig. S2† illustrating a monotonic increase in Si atomic percentage with the number of ALD cycles. High-resolution Si 2p spectra indicated that the Si in the coated samples predominantly exists in the SiO_2 state, which can be deconvoluted into Si 2p3/2 and Si 2p1/2 peaks. This demonstrated successful SiO_2 deposition on the surface of Ag/CB samples, with the Si content increasing proportionally with the number of coating cycles.

This journal is © The Royal Society of Chemistry 2025

Catal. Sci. Technol., 2025, **15**, 2148–2159 | **2151**

The stability of the original Ag/CB catalyst was assessed in an H-cell at −1.0 V *vs.* RHE over a 20 hour period. Fig. 2 shows that the Faradaic efficiency (FE) of the original Ag/CB catalyst towards CO remained relatively constant at around 70% throughout the 20 hour test, with minor fluctuations. The total Faradaic efficiency falling below 100% can be attributed to incomplete product detection and electron losses resulting from parasitic processes, such as electrode corrosion and catalyst degradation. This underscores the stability of the original Ag/CB catalyst in H-cell environments, consistent with previous research, indicating the robustness of Ag catalysts under similar testing conditions.[2–5] Notably, the Ag catalyst exhibited no significant deterioration in performance under neutral pH conditions. However, the selectivity of the original Ag catalyst was found to be lower than that reported in some papers.[2,33,34] To further investigate the selectivity of the Ag catalyst, we also evaluated pure Ag nanoparticles drop-casted onto a glassy carbon electrode while maintaining consistent metal loading (80 μg cm^{-2}) with our Ag/CB catalyst. As depicted in Fig. S3,† an optimal FE$_{CO}$ of the pure Ag nanoparticles was achieved at −0.8 V *vs.* RHE, with a similar selectivity towards CO of around 70%. Upon mixing the Ag nanoparticles with carbon black to mimic our Ag/CB catalyst while keep the same Ag loading on the electrode, we observed that the optimal FE was achieved at −1.0 V *vs.* RHE, demonstrating a FE$_{CO}$ of approximately 72%. This indicated that the low FE of the Ag catalyst was not inherent to the catalyst itself but was more associated with the used H-cell configuration. In the H-cell configuration, the availability of CO$_2$ in the cathode compartment was restricted due to the low solubility of CO$_2$ in the electrolyte. The low solubility of CO$_2$ resulted in a low concentration of CO$_2$ in the vicinity of the electrode. When the CO$_2$ concentration near the cathode is insufficient, the FE$_{CO}$ decreases. CO$_2$ must then diffuse through the electrolyte to reach the cathode, and in the H-cell configuration, this diffusion is hindered by the distance between the CO$_2$ source (*e.g.*, the gas phase or CO$_2$ inlet) and the cathode. The slower diffusion rate can lead to localized CO$_2$ depletion at the electrode, further restricting CO$_2$ reduction efficiency. Mass transfer, including the movement of CO$_2$ to the electrode, is also limited in the H-cell configuration due to the static nature of the electrolyte and the lack of continuous flow. These limitations were more serious under high current densities, as these conditions require a higher amount of CO$_2$ supply. Consequently, CO$_2$ reduction in the H-cell was less efficient, resulting in lower FE towards CO. While the partial current density of the Ag nanoparticles with or without mixing with carbon black towards CO appeared comparable at all three potentials, there was a notable disparity in the H$_2$ partial current density between the Ag nanoparticles drop casted directly on the glassy carbon electrode and those mixed with carbon black. The Ag nanoparticles mixed with carbon black consistently exhibited a lower H$_2$ partial current density at all three potentials. We hypothesize that part of the Ag is buried beneath the carbon particles. This means that the CO$_2$ consumption during CO$_2$ reduction will be lower with these samples. Therefore, the samples with carbon black will have a relatively higher CO$_2$ concentration near the electrode, which suppresses the hydrogen evolution activity.

SO$_2$ concentrations of 10 ppm, 100 ppm, and 1000 ppm were tested in this study, considering that the majority of flue gas
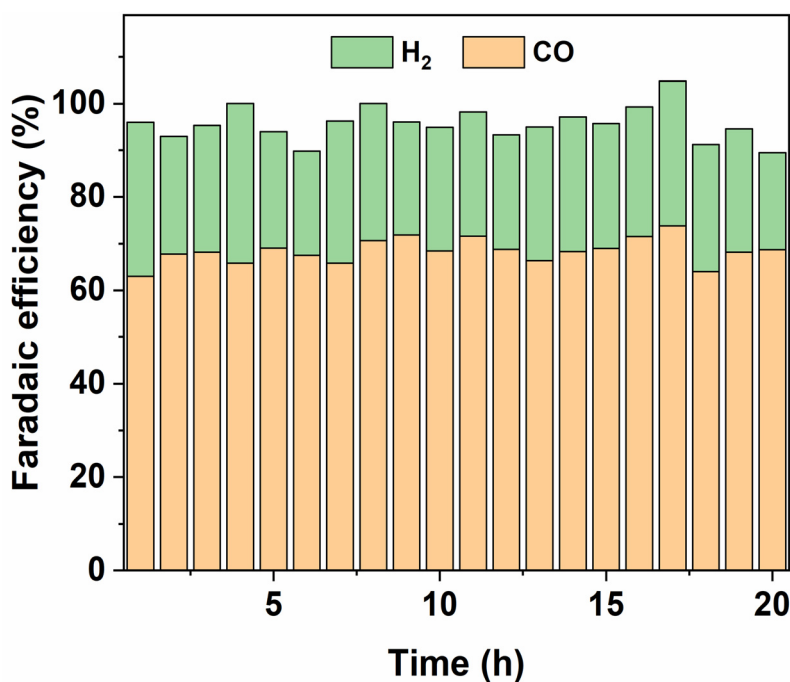

Fig. 2 Faradaic efficiency toward H$_2$ and CO of the uncoated Ag/CB catalyst during 20 h H-cell testing at −1.0 V *vs.* RHE using a pure CO$_2$ gas feed and a 0.1 M KHCO$_3$ electrolyte.

2152 | *Catal. Sci. Technol.*, 2025, **15**, 2148–2159

This journal is © The Royal Society of Chemistry 2025

emissions from power plants typically fall within an SO_2 concentration range from 100 to 400 ppm.[18] The gas compositions employed for the SO_2 impurity experiments are listed in Table S2.† Three different CO_2 gas cylinders containing 0, 100, and 10 000 ppm SO_2 were utilized, and a gas mixer was employed to ensure thorough mixing of various gas streams to achieve a homogeneous gas stream flowing into the H-cell cathode chamber. The original Ag/CB catalyst (*i.e.*, 0 cycles) and catalysts with 2, 4 and 8 cycles of SiO_2 ALD coating were tested at three potentials using chronoamperometry (CA) under different gas feed compositions. As is seen from Fig. 3, the catalyst performance was first benchmarked with a pure CO_2 feed and a similar selectivity toward CO was observed with and without SiO_2 coating, reaching the highest FE_{CO} of 70% at −1.0 V *vs.* RHE. Nevertheless, when SO_2 impurities were introduced into the gas stream, the FE_{CO} of the uncoated Ag/CB catalyst showed a significant decrease. A decrease in FE_{CO} to 57% with 10 ppm SO_2 and 56% with 100 ppm SO_2, at −1.0 V *vs.* RHE was observed. At the highest SO_2 concentration (1000 ppm), the FE_{CO} decreased by 23%, 24%, and 14% at −0.8 V *vs.* RHE, −1.0 V *vs.* RHE, and −1.2 V *vs.* RHE, respectively. The SO_2 poisoning effect on the Ag catalyst appears to be potential dependent, with a greater impact observed at lower potentials. This is expected due to the more favorable reduction of SO_2 over CO_2, since SO_2 reduction has a significantly less negative reduction potential compared to CO_2 reduction.[35] We have conducted cyclic voltammetry tests under various gas supplies, including pure Ar, CO_2 with 1000 ppm SO_2 and pure CO_2 to verify the CO_2 reduction potential and the SO_2 reduction potential. However,

as shown in Fig. S4,† no distinct SO_2 reduction peak was observed. This indicates that SO_2 reduction occurs within a potential window similar to that of CO_2 reduction and hydrogen evolution. When we calculate the loss in FE_{CO} and attribute it to SO_2 reduction, we find that approximately 50 ppm SO_2 is required to account for the missing FE when 1000 ppm SO_2 is introduced at −0.8 V *vs.* RHE. This suggests that there is sufficient SO_2 in the gas stream during the reaction for the indicated SO_2 reduction (detailed calculation method can be found in ESI,† method to calculate the SO_2 concentration required to get SO_2 reduction section). Additionally, the potential poisoning of the Ag/CB catalyst during the reaction can also contribute to the performance degradation when SO_2 is introduced to the gas stream, as we detected the formation of Ag_2S species on the surface of the catalyst after the reaction, as shown in Fig. 4. Although the exact mechanism of the Ag_2S formation process is unclear and remains an objective for future study. All of these factors combined together contribute to the decrease in FE_{CO} for the CO_2 electrolysis. The decrease in CO selectivity of the Ag/CB catalyst at a high concentration of SO_2 impurities was more pronounced at less negative potential (−0.8 V *vs.* RHE) compared to more negative potential (−1.2 V *vs.* RHE) indicating that the competition between SO_2 reduction and CO_2 reduction is potential dependent. SO_2 reduction is more favored compared to CO_2 reduction at less negative potentials. As the potential becomes more negative, the effectiveness of CO_2 reduction increases, with the loss in FE_{CO} decreasing. The Ag/CB catalysts protected with 2–8 ALD cycles of SiO_2 coating were much less affected by the SO_2
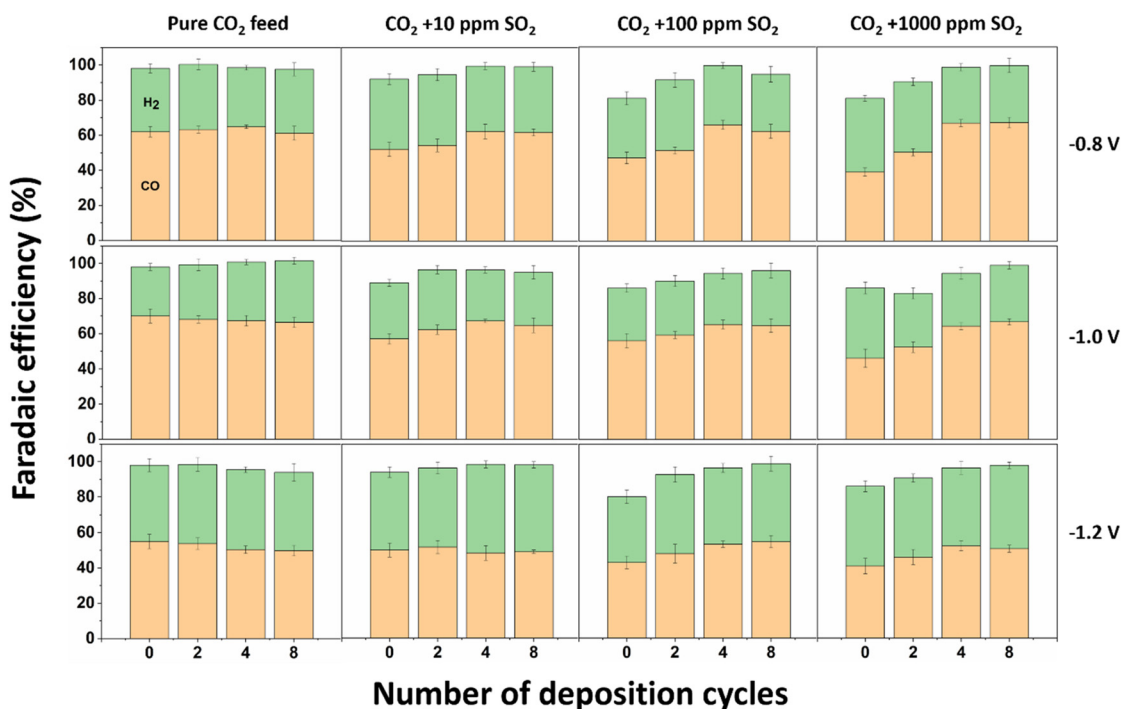

Fig. 3 Faradaic efficiency of the Ag/CB catalyst with or without SiO_2 coating during 1 h H-cell CA testing in a 0.1 M $KHCO_3$ electrolyte at 3 potentials using CO_2 gas feed with different concentrations of SO_2 impurities. The data was collected from two independent measurements and the error bars represent the arithmetic mean.
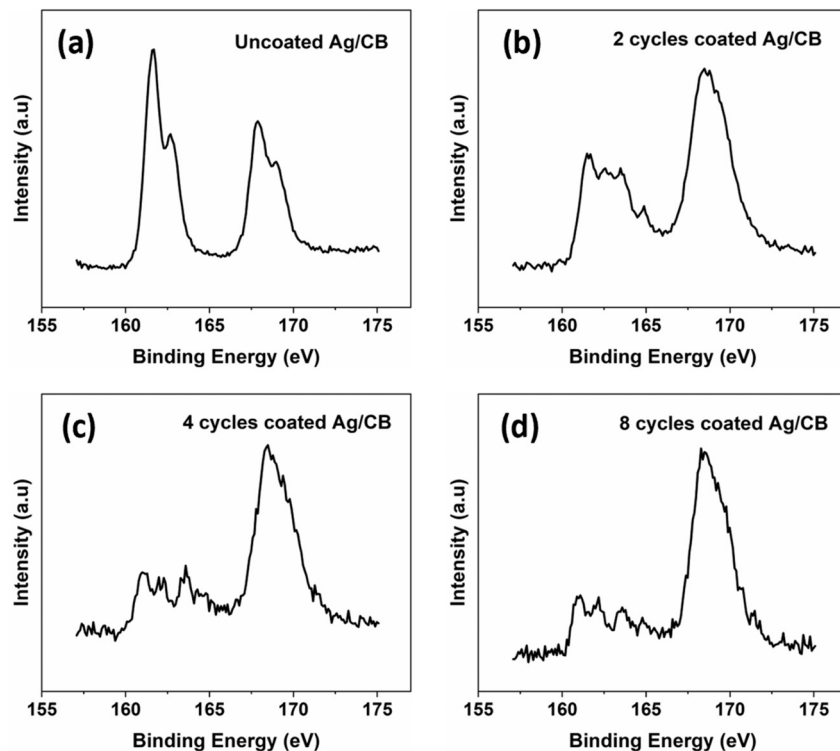
This journal is © The Royal Society of Chemistry 2025

Catal. Sci. Technol., 2025, **15**, 2148–2159 | **2153**

Fig. 4 S 2p XPS spectrum of the Ag/CB catalyst after CO_2 electrolysis with 1000 ppm SO_2. (a) Ag/CB catalyst without SiO_2 coating. (b) Ag/CB catalyst with 2 cycles SiO_2 coating. (c) Ag/CB catalyst with 4 cycles SiO_2 coating. (d) Ag/CB catalyst with 8 cycles SiO_2 coating, tested at H-cell at −1.0 V *vs.* RHE.

contaminant. At −0.8 V *vs.* RHE, the FE_{CO} of the uncoated Ag/CB catalyst was 52%, 47%, and 39% with 10 ppm SO_2, 100 ppm SO_2, and 1000 ppm SO_2, respectively. After applying 2 cycles of SiO_2 coating on the surface of the catalyst, the FE_{CO} improved to 54%, 51%, and 50%, respectively. When we further increased the coating cycles to 4 cycles, the FE_{CO} of the ALD coated catalyst increased to 62%, 65%, and 66%. After 8 cycles of SiO_2 coating, the FE_{CO} reached 62%, 62%, and 67%. The SiO_2 coating thereby effectively reduced the SO_2 poisoning effect on the Ag catalyst. When the applied potential became more negative, the SO_2 effects on Ag catalyst decreased, and the coating effectiveness decreased as well. The FE_{CO} of the uncoated Ag/CB catalyst at −1.2 V *vs.* RHE was 50%, 43%, and 41% under 10 ppm SO_2, 100 ppm SO_2, and 1000 ppm SO_2, respectively. After 2 cycles of coating, the FE_{CO} improved to 51%, 48%, and 46%. And after 4 cycles coating, it increased to 48%, 53%, and 52%. With 8 cycles coating, the FE_{CO} improved to 49%, 54%, and 50%. The decreased FE_{CO}, especially for the uncoated and 2 cycles coated samples under SO_2 impurity, can likely be attributed to the SO_2 reduction and the poisoning of the catalysts. However, due to the high solubility of the sulfur-containing anions in the electrolyte and its cross-over through the anion-exchange membrane to the anolyte, we cannot accurately detect the SO_2 reduction products and quantify their Faradaic efficiency.

Fig. 4 presents the XPS characterization of the Ag/CB catalyst without and with SiO_2 coating following a 1 hour CA test at −1.0 V *vs.* RHE with 1000 ppm SO_2. In all samples, an intense peak at 168.7 eV was observed in the S 2p spectrum, attributed to the sulfur-containing functional groups within the Nafion binder

utilized for drop-casting the catalyst on the surface of the glassy carbon electrode, and serving as the ionomer in the catalyst. Peaks at 161.1 eV and 162.2 eV are attributed to silver sulfide (Ag_2S) formation during the reaction.[36] Notably, the intensity of the Ag_2S peaks was notably higher in the uncoated catalyst. Upon applying 2–8 cycles of SiO_2 coating, a decrease in the intensity of the Ag_2S peak was observed, suggesting that SiO_2 coating mitigated Ag_2S formation during the reaction under high concentrations of SO_2 (1000 ppm SO_2) gas feed. An XPS area scan was conducted after 1 h CO_2 electrolysis at −1.0 V *vs.* RHE with 2 kinds of gas feed. Fig. S5† shows that the uncoated Ag/CB catalyst after 1 h CO_2 electrolysis with pure CO_2 gas feed only has a low intensity of S peak on the electrode. For a gas feed of CO_2 with 1000 ppm SO_2, the uncoated Ag/CB catalyst shows a much stronger S peak on the electrode. Nevertheless, for the catalyst treated with 8 cycles of SiO_2 coating, the S peak is significantly decreased on the electrode after CO_2 electrolysis with 1000 ppm SO_2.

In summary, we found that the Ag/CB catalyst was significantly affected by SO_2 impurities in the H-cell geometry, especially for a high SO_2 concentration and at a less negative potential. The SiO_2 coating can be used to protect the Ag/CB catalyst from SO_2 impurities and maintain the catalyst selectivity for all investigated potentials.

SO_2 and CO_2 permeability differences through SiO_2 coating

To further illustrate the protection mechanism of SiO_2 on Ag/CB catalysts against SO_2 impurities, we investigated the

2154 | *Catal. Sci. Technol.*, 2025, **15**, 2148–2159

This journal is © The Royal Society of Chemistry 2025

permeability differences of SO_2 and CO_2 through SiO_2 coatings based on existing papers. Mohd Nor *et al.* found that CO_2 has high permeability through SiO_2 modified polymer matrix membranes.[37] After adding 5 wt% of SiO_2 nanoparticles to the polymer matrix membranes (ENR/PVC), the CO_2 gas permeability increased to approximately 6 times higher than the original membranes without SiO_2 modification. Wahab *et al.* also found a similar phenomenon.[38] They reported that CO_2 gas exhibits strong interaction with SiO_2 due to the presence of hydroxyl functional groups (–OH) on the SiO_2 particles. This interaction enhances the solubility of CO_2 within the membrane, thereby improving CO_2 diffusivity and resulting in high permeability of CO_2 through SiO_2 filled fiber mixed matrix membrane. Meng *et al.* tested that the organic–inorganic hybrid SiO_2 membranes exhibited a high O_2 permeance that was 2.87×10^{-8} mol m^{-2} s^{-1} Pa^{-1} and a poor SO_2 permeance of 3.9×10^{-9} mol m^{-2} s^{-1} Pa^{-1}.[39] The O_2 permeance was 7.4 times higher than the SO_2 permeance through the membranes. This indicates that the SO_2 permeability through this organic–inorganic hybrid SiO_2 membranes is very low. Yoshiura *et al.* also found that the 3,3,3-trifluoropropyltrimethoxysilane derived SiO_2 membranes have very high SO_4^{2-} ions rejection rates.[40] The $NaSO_4$ and $MgSO_4$ rejection percentage after the liquid permeation tests was 91.0% and 98.2%, respectively. This is attributed to the dissociation of the –OH groups on the silica surface during testing and produce a negatively charged surface. The SiO_2 coating on the Ag/CB catalyst was negatively charged during CO_2RR as well. Hence, it can also have a repulsive effect on SO_2 derived ions. Yu *et al.* discovered that silica–zirconia membranes with a high Si/Zr molar ratio (Si/Zr = 7/3) exhibit excellent resistance to SO_3 and demonstrate gas separation of O_2/SO_3 selectivity ranging from 13 to 10, surpassing the Knudsen selectivity of 1.58.[41] This suggests promising potential for their application in O_2/SO_3 separation processes and indicates that O_2 has more than 10 times higher permeability through silica–zirconia membranes with a high Si/Zr molar ratio compared to SO_3. Based on the preceding discussion, it can be inferred that there is a notable difference in the permeability of CO_2 and SO_2 through SiO_2, with CO_2 showing significantly higher permeability compared to SO_2 or SO_2 derived ions present in the electrolyte. The variation in permeability between CO_2 and SO_2 indicates that the concentrations of these gases outside and inside the SiO_2 coating, which directly interact with the Ag/CB catalyst, are also likely to differ. The lower SO_2 concentration on the inside of the coating may account for the observation that after applying 2–8 cycles of SiO_2 coating, the formation of Ag_2S on the electrode surface is considerably less than without SiO_2 coating after CO_2 electrolysis with 1000 ppm SO_2 feed at −1.0 V *vs.* RHE. It also explains why SO_2 has much less effect on the catalyst's selectivity after it has been coated with SiO_2 films. The SO_2 concentration near the electrode surface decreases, so the competition between the SO_2 reduction and CO_2 reduction is

reduced, and the potential poisoning of the Ag/CB catalyst is minimized.

SO_2 impurities effects on CO_2 electroreduction in MEA reactor

Based on the findings from our investigation using the H-cell, we proceeded to evaluate the performance of SiO_2 coated Ag/CB samples in a MEA reactor, a widely utilized flow cell structure in the field of CO_2 reduction, to understand their behavior in the flow cell system. Given that the current density in the H-cell is relatively low and cannot meet industrially relevant requirements, assessing the SiO_2 coated Ag/CB catalyst in a flow cell geometry such as a MEA is needed.

We applied 4 cycles of SiO_2 coating on Ag/CB powders using a fluidized bed ALD reactor. This is different from the samples used in H-cell tests, in which we used a flat substrate ALD reactor and only coated the very outermost surface of the Ag/CB catalyst on the glassy carbon electrode. For these experiments, we fluidized the Ag/CB powder in a dedicated ALD reactor and coated the entire surface of the Ag/CB particles. The coated Ag/CB catalyst was airbrushed on the gas diffusion electrode and assembled in the MEA electrolyzer for the electrochemistry tests. The uncoated Ag/CB catalyst tested in MEA showed a FE_{CO} of 79% at 100 mA cm^{-2} with a pure CO_2 gas feed (as shown in Fig. 5a). When the gas feed shifted to CO_2 with 1000 ppm SO_2, the FE_{CO} did not decrease significantly as in the experiments in the H-cell, but remained at a FE_{CO} of 75%. When the Ag/CB catalyst was coated with 4 cycles of SiO_2, we observed that the catalyst's selectivity was inhibited to some extent. The 4 cycles SiO_2 coated sample showed a FE_{CO} of 70% with pure CO_2 feed, and a FE_{CO} of 71% when the gas feed was changed to CO_2 combined with 1000 ppm SO_2. The slight inhibition effect of the coating may stem from the SiO_2 coating forming connections between catalyst particles, which could hinder electrical conductivity and ionic charge transfer between the membrane and the bulk catalyst. The water transport within the bulk catalyst might also be influenced by the SiO_2 coating. All of these factors can collectively affect the catalyst's selectivity in the MEA configuration. Fig. S6† shows that the CV scan of the uncoated Ag/CB catalyst and the catalyst with 4 cycles of SiO_2 coating do not have notable differences. The oxidation and reduction peaks of Ag are well defined with 4 cycles of SiO_2 coating and nearly coincide with the catalyst without coating. This indicates that the obstruction caused by the SiO_2 coating on the catalyst's outmost surface active sites is minimal. Fig. 5b and c shows the chronopotentiometry (CP) results of the Ag/CB catalyst tested at 100 mA cm^{-2}. It indicates that adding 1000 ppm SO_2 to the feeding gas does not change the cell potential under the same current density. Applying an SiO_2 coating also did not alter the cell potential for the same current density. The XPS characterization of the catalyst before and after CO_2 electrolysis with or without SO_2 impurities are
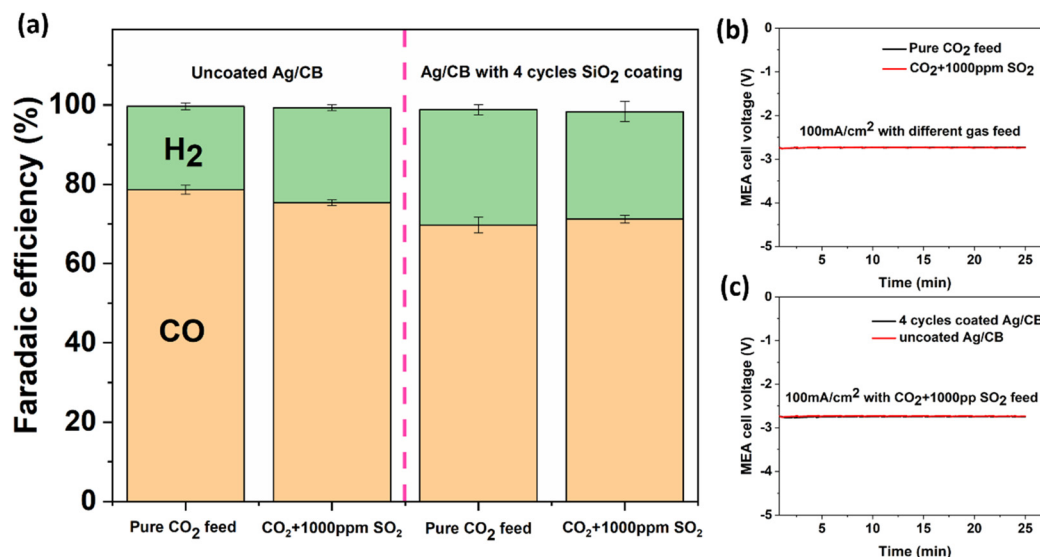
Fig. 5 (a) Faradaic efficiency of the Ag/CB catalyst with or without SiO_2 coating tested at MEA reactor at 100 mA cm^{-2} current density in a 1 M $KHCO_3$ electrolyte with pure CO_2 feed or CO_2 mixed with 1000 ppm SO_2. The data was collected from two independent measurements and the error bars represent the arithmetic mean. (b) CP testing of the Ag/CB catalyst at MEA reactor. Original Ag/CB catalyst tested with pure CO_2 or CO_2 with 1000 ppm SO_2 impurities at 100 mA cm^{-2} current density. (c) CP testing of the Ag/CB catalyst at MEA reactor. Ag/CB catalyst with or without 4 cycles of SiO_2 coating tested using CO_2 with 1000 ppm SO_2 impurities as gas feed at 100 mA cm^{-2} current density.

shown in Fig. 6. From the figure we observe that peaks at 161.1 eV and 162.2 eV, which are attributed to Ag_2S, are present in all samples, even with pure CO_2 feed. This is likely due to the higher Nafion loading on the GDE (218.5 μg cm^{-2}) compared to the H-cell electrode (87.4 μg cm^{-2}), and more importantly, the higher current density in MEA caused more reduction of sulfonic acid ($-SO_3H$) groups in the Nafion binder during CO_2 electrolysis. We can observe that the Ag_2S
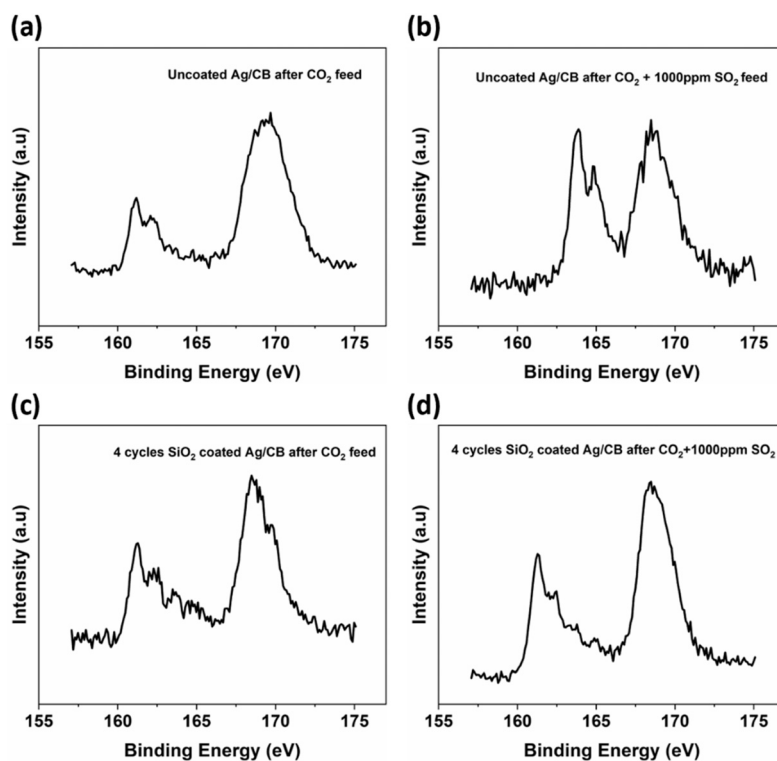

Fig. 6 S 2p XPS spectrum of the Ag/CB catalyst after CO_2 electrolysis tested at MEA reactor at 100 mA cm^{-2}. (a) Ag/CB catalyst tested with CO_2 feed. (b) Ag/CB catalyst tested with CO_2 + 1000 ppm SO_2 feed. (c) Ag/CB catalyst with 4 cycles SiO_2 coating tested with CO_2 feed. (d) Ag/CB catalyst with 4 cycles SiO_2 coating tested with CO_2 + 1000 ppm SO_2 feed.

peak becomes stronger after shifting the feed gas from pure CO_2 to CO_2 combined with 1000 ppm SO_2 for the catalyst without SiO_2 coating. Nevertheless, for the catalyst coated with 4 cycles of SiO_2, the Ag_2S peak remains almost identical with or without 1000 ppm SO_2 in the feed gas stream. This suggests that inhibition of SO_2 penetration by SiO_2 is also present in the MEA experiments.

SO_2 impurities in the CO_2 feed had a stronger influence on Ag/CB catalysts within the H-cell system than in the MEA reactor under the conditions used here. We attribute this difference in behaviour to the higher solubility of SO_2 in the liquid electrolyte compared to CO_2, resulting in an accumulation of SO_2 in the batchwise operated H-cell, but not in the MEA flow cell configuration. A visual representation of both cell geometries is provided in Fig. S7.† The solubility of CO_2 in water at 20 °C is 1.7 g L^{-1}. Under the same conditions, the solubility of SO_2 is 110 g L^{-1}, nearly 65 times higher than that of CO_2 in the electrolyte. This will lead to a continuous increase of SO_2 concentration in the electrolyte within the H-cell during the experiments until it reaches saturation. However, due to the high solubility of SO_2 in the electrolyte and the relatively low concentration of SO_2 in the feed gas stream, even with the highest concentration of SO_2 used in the experiments (CO_2 with 1000 ppm SO_2, which means 0.1 vol% of SO_2 in the CO_2 stream), it would require 6.6 days of continuous dosing to reach SO_2 saturation in the electrolyte. This implies that the electrolyte will never reach saturation during the H-cell experiments and the SO_2 concentration in the electrolyte will keep on increasing during the experiments. Consequently, the SO_2 concentration near the surface of the electrode will be much higher than in the feed gas for the H-cell experiments. On the contrary, in the MEA reactor geometry, the cathode is in direct contact with the feed gas, without the presence of electrolyte in the cathode serpentine channel. Therefore, the SO_2 concentration near the cathode in the MEA system is the same as in the feed gas, which is much lower than the concentration near the cathode in the H-cell system with the same feed gas composition. This explains why the Ag/CB catalyst in the MEA system is not significantly affected by SO_2 impurities and it shows that the Ag/CB catalyst can maintain its performance with 1000 ppm SO_2 impurities in the MEA system within our 25 minutes testing timeframe. The long-term stability of the Ag/CB catalyst in the MEA reactor under SO_2 impurities is worth investigating as well. However, after 50 minutes of CP testing, we encountered significant salt precipitation in the MEA system, resulting in a subsequent decrease in Faradaic efficiency. The first 18 minutes serve as a stabilization period, during which the reaction products are transferred to the GC. During this period, the Faradaic efficiency for both H_2 and CO is lower than expected. Additionally, the FE_{CO} started to decrease after 35 minutes during CP testing with pure CO_2 gas feed at 100 mA cm^{-2}, as shown in Fig. S8.† Very obvious $KHCO_3$ salt precipitation can be seen on the cathode serpentine channel and gas diffusion electrode after 50 minutes CP testing (as shown in Fig. S9†).

Nevertheless, the cell potential was relatively stable during 50 minutes CP testing, as can be seen in Fig. S10.† The minor fluctuation was due to the gas chromatography (GC) injection during the CP testing. Salt precipitation issues prevented us from further investigating the stability of Ag/CB catalyst in the MEA system, especially in the presence of SO_2 impurities. Therefore, this research question awaits further investigation in subsequent studies.

Conclusions

We have explored the performance of the Ag/CB catalyst under SO_2 impurities for CO_2 electrolysis in two electrochemical cell geometries: an H-cell and a MEA cell. Both systems behave differently with respect to SO_2 contamination in the CO_2 feed. The impact of SO_2 on Ag/CB catalysts was large in the H-cell, while it was nearly absent in the MEA geometry under the relatively short testing time used in this study. This difference can be attributed to the greater solubility of SO_2 in the electrolyte compared to CO_2, leading to an accumulation effect and a much higher liquid phase concentration of SO_2 in the H-cell. This led to a greater performance decrease of the Ag/CB catalyst in the H-cell compared to the MEA geometry, when exposed to the same concentration of SO_2 impurities. An ultrathin SiO_2 coating synthesized *via* ALD protected the Ag/CB catalyst in the H-cell against SO_2 impurities under relatively less negative potentials. This is due to the SO_2 and CO_2 permeability differences through the SiO_2 coatings. CO_2 has much higher permeability compared to SO_2 (or SO_2 derived ions) through SiO_2. This leads to a significant obstruction in the interaction of SO_2 with the catalyst and might decrease the SO_2 concentration after the SiO_2 coatings.

Data availability

The data supporting this article have been included as part of the ESI† see DOI: **https://doi.org/10.1039/D4CY01196A**.

Author contributions

M. Li: conceptualization, methodology, formal analysis, validation, writing – original draft. S. Fu: methodology, validation, writing – review & editing. R. Kortlever: supervision, writing – review & editing, project administration. J. R. van Ommen: supervision, writing – review & editing, project administration, funding acquisition.

Conflicts of interest

J. R. van Ommen has a financial interest in Powall.

Acknowledgements

This journal is © The Royal Society of Chemistry 2025

Catal. Sci. Technol., 2025, **15**, 2148–2159 | **2157**

assistance in the lab, Bart Boshuizen for the XPS area scan training and Baukje Terpstra for the ICP-OES analysis.

Notes and references

1 C. Chen, J. F. Khosrowabadi Kotyk and S. W. Sheehan, Progress toward Commercial Application of Electrochemical Carbon Dioxide Reduction, *Chem*, 2018, **4**(11), 2571–2586.

2 M. Ma, K. Liu, J. Shen, R. Kas and W. A. Smith, In Situ Fabrication and Reactivation of Highly Selective and Stable Ag Catalysts for Electrochemical CO$_2$ Conversion, *ACS Energy Lett.*, 2018, **3**(6), 1301–1306.

3 N. Zhang, X. Zhang, L. Tao, P. Jiang, C. Ye and R. Lin, *et al.* Silver Single-Atom Catalyst for Efficient Electrochemical CO$_2$ Reduction Synthesized from Thermal Transformation and Surface Reconstruction, *Angew. Chem., Int. Ed.*, 2021, **60**(11), 6170–6176.

4 H. Wang, Z. Han, L. Zhang, C. Cui, X. Zhu and X. Liu, *et al.* Enhanced CO selectivity and stability for electrocatalytic reduction of CO$_2$ on electrodeposited nanostructured porous Ag electrode, *J. CO2 Util.*, 2016, **15**, 41–49.

5 S.-Q. Liu, S.-W. Wu, M.-R. Gao, M.-S. Li, X.-Z. Fu and J.-L. Luo, Hollow Porous Ag Spherical Catalysts for Highly Efficient and Selective Electrocatalytic Reduction of CO$_2$ to CO, *ACS Sustainable Chem. Eng.*, 2019, **7**(17), 14443–14450.

6 J. Osiewacz, M. Löffelholz, L. Weseler and T. Turek, CO poisoning of silver gas diffusion electrodes in electrochemical CO$_2$ reduction, *Electrochim. Acta*, 2023, **445**, 142046.

7 D. E. Doronkin, T. S. Khan, T. Bligaard, S. Fogel, P. Gabrielsson and S. Dahl, Sulfur poisoning and regeneration of the Ag/γ-Al$_2$O$_3$ catalyst for H$_2$-assisted SCR of NO$_x$ by ammonia, *Appl. Catal., B*, 2012, **117–118**, 49–58.

8 F. Gobal and L. Majari Kasmaee, Polysulfide Poisoning of Ag Electrocatalyst during L-Ascorbate Ion Electro-oxidation in Alkaline Solution, *Chin. J. Catal.*, 2012, **33**(2–3), 267–274.

9 V. Houel, P. Millington, S. Pollington, S. Poulston, R. R. Rajaram and A. Tsolakis, Chemical deactivation of Ag/Al$_2$O$_3$ by sulphur for the selective reduction of NO$_x$ using hydrocarbons, *Catal. Today*, 2006, **114**(4), 334–339.

10 P. Bains, P. Psarras and J. Wilcox, CO$_2$ capture from the industry sector, *Prog. Energy Combust. Sci.*, 2017, **63**, 146–172.

11 T. Al-Attas, S. K. Nabil, A. S. Zeraati, H. S. Shiran, T. Alkayyali and M. Zargartalebi, *et al.* Permselective MOF-Based Gas Diffusion Electrode for Direct Conversion of CO$_2$ from Quasi Flue Gas, *ACS Energy Lett.*, 2022, **8**(1), 107–115.

12 G. Pipitone and O. Bolland, Power generation with CO$_2$ capture: Technology for CO$_2$ purification, *Int. J. Greenhouse Gas Control*, 2009, **3**(5), 528–534.

13 R. T. J. Porter, M. Fairweather, M. Pourkashanian and R. M. Woolley, The range and level of impurities in CO$_2$ streams from different carbon capture sources, *Int. J. Greenhouse Gas Control*, 2015, **36**, 161–174.

14 D. M. D'Alessandro, B. Smit and J. R. Long, Carbon dioxide capture: prospects for new materials, *Angew. Chem., Int. Ed.*, 2010, **49**(35), 6058–6082.

15 G. V. Last and M. T. Schmick, *Identification and Selection of Major Carbon Dioxide Stream Compositions*, US Department of Energy, 2011, PNNL-20493.

16 B. H. Ko, B. Hasa, H. Shin, E. Jeng, S. Overa and W. Chen, *et al.* The impact of nitrogen oxides on electrochemical carbon dioxide reduction, *Nat. Commun.*, 2020, **11**(1), 5856.

17 Y. Xu, J. P. Edwards, J. Zhong, C. P. O'Brien, C. M. Gabardo and C. McCallum, *et al.* Oxygen-tolerant electroproduction of C2 products from simulated flue gas, *Energy Environ. Sci.*, 2020, **13**(2), 554–561.

18 S. Van Daele, L. Hintjens, S. Hoekx, B. Bohlen, S. Neukermans and N. Daems, *et al.* How flue gas impurities affect the electrochemical reduction of CO$_2$ to CO and formate, *Appl. Catal., B*, 2024, **341**, 123345.

19 P. P. Albertini, M. A. Newton, M. Wang, O. Segura Lecina, P. B. Green and D. C. Stoian, *et al.* Hybrid oxide coatings generate stable Cu catalysts for CO$_2$ electroreduction, *Nat. Mater.*, 2024, **23**(5), 680–687.

20 H. Van Bui, F. Grillo and J. R. van Ommen, Atomic and molecular layer deposition: off the beaten track, *Chem. Commun.*, 2016, **53**(1), 45–71.

21 K. S. Yoo, D.-G. Kim, S. Lee, W.-B. Lee and J.-S. Park, Atmospheric pressure spatial ALD of Al$_2$O$_3$ thin films for flexible PEALD IGZO TFT application, *Ceram. Int.*, 2022, **48**(13), 18803–18810.

22 D. H. Levy, D. Freeman, S. F. Nelson, P. J. Cowdery-Corvan and L. M. Irving, Stable ZnO thin film transistors by fast open air atomic layer deposition, *Appl. Phys. Lett.*, 2008, **92**, 192101.

23 D. La Zara, F. Sun, F. Zhang, F. Franek, K. Balogh Sivars and J. Horndahl, *et al.* Controlled Pulmonary Delivery of Carrier-Free Budesonide Dry Powder by Atomic Layer Deposition, *ACS Nano*, 2021, **15**(4), 6684–6698.

24 J. W. Klaus and S. M. George, Atomic layer deposition of SiO$_2$ at room temperature using NH$_3$-catalyzed sequential surface reactions, *Surf. Sci.*, 1999, **447**(2000), 81–90.

25 F. Grillo, H. Van Bui, J. A. Moulijn, M. T. Kreutzer and J. R. van Ommen, Understanding and Controlling the Aggregative Growth of Platinum Nanoparticles in Atomic Layer Deposition: An Avenue to Size Selection, *J. Phys. Chem. Lett.*, 2017, **8**(5), 975–983.

26 M. Li, S. Fu, S. Saedy, A. Rajendrakumar, F. D. Tichelaar and R. Kortlever, *et al.* Nanostructuring Pt-Pd Bimetallic Electrocatalysts for CO$_2$ Reduction Using Atmospheric Pressure Atomic Layer Deposition, *ChemCatChem*, 2022, **14**, e202200949.

27 R. Kamphorst, P. Wanjari, S. Saedy, J. F. K. van Dam, A. Thijssen and P. Brüner, *et al.* Enhancing colloid stability of polymer microspheres in water through SiO$_2$ coating: Effects of coating cycles and surface coverage, *Surf. Interfaces*, 2024, **45**, 103852.

28 Y. Song and P. N. Pintauro, The electrochemical synthesis of aminonitriles I. H-cell studies with adiponitrile and azelanitrile, *J. Appl. Electrochem.*, 1991, **21**, 21–27.

29 L. Wang, C.-Y. Lee and P. Schmuki, Solar water splitting: preserving the beneficial small feature size in porous α-Fe$_2$O$_3$ photoelectrodes during annealing, *J. Mater. Chem. A*, 2013, **1**(2), 212–215.

2158 | *Catal. Sci. Technol.*, 2025, **15**, 2148–2159

This journal is © The Royal Society of Chemistry 2025

30 M. Li, S. Saedy, S. Fu, T. Stellema, R. Kortlever and J. R. van Ommen, Enhancing the durability of Pt nanoparticles for water electrolysis using ultrathin SiO_2 layers, *Catal. Sci. Technol.*, 2024, **14**(5), 1328–1335.

31 Y. Du, X. Du and S. M. George, SiO2 film growth at low temperatures by catalyzed atomic layer deposition in a viscous flow reactor, *Thin Solid Films*, 2005, **491**(1–2), 43–53.

32 J. W. Klaus, O. Sneh and S. M. George, Growth of SiO_2 at Room Temperature with the Use of Catalyzed Sequential Half-Reactions, *Science*, 1997, **278**(5345), 1934–1936.

33 H. Yun, J. Kim, W. Choi, M. H. Han, J. H. Park and H.-S. Oh, *et al.* Understanding morphological degradation of Ag nanoparticle during electrochemical CO_2 reduction reaction by identical location observation, *Electrochim. Acta*, 2021, **371**, 137795.

34 C. Kim, T. Eom, M. S. Jee, H. Jung, H. Kim and B. K. Min, *et al.* Insight into Electrochemical CO_2 Reduction on Surface-Molecule-Mediated Ag Nanoparticles, *ACS Catal.*, 2016, **7**(1), 779–785.

35 N. J. Harmon and H. Wang, Electrochemical CO_2 Reduction in the Presence of Impurities: Influences and Mitigation Strategies, *Angew. Chem., Int. Ed.*, 2022, **61**(52), e202213782.

36 S. Ghafoor, S. Ata, N. Mahmood and S. N. Arshad, Photosensitization of TiO_2 nanofibers by Ag_2S with the synergistic effect of excess surface Ti^{3+} states for enhanced photocatalytic activity under simulated sunlight, *Sci. Rep.*, 2017, **7**(1), 255.

37 F. M. Nor, N. H. A. Karim, I. Abdullah and R. Othaman, Permeability of carbon dioxide and nitrogen gases through SiO_2 and MgO incorporated ENR/PVC membranes, *J. Elastomers Plast.*, 2016, **48**(6), 483–498.

38 M. F. A. Wahab, A. F. Ismail and S. J. Shilton, Studies on gas permeation performance of asymmetric polysulfone hollow fiber mixed matrix membranes using nanosized fumed silica as fillers, *Sep. Purif. Technol.*, 2012, **86**, 41–48.

39 L. Meng, M. Kanezashi, J. Wang and T. Tsuru, Permeation properties of BTESE–TEOS organosilica membranes and application to O_2/SO_2 gas separation, *J. Membr. Sci.*, 2015, **496**, 211–218.

40 J. Yoshiura, K. Ishii, Y. Saito, T. Nagataki, Y. Nagataki and A. Ikeda, *et al.* Permeation Properties of Ions through Inorganic Silica-Based Membranes, *Membranes*, 2020, **10**, 27.

41 X. Yu, L. Meng, H. Nagasawa, M. Kanezashi, M. Machida and T. Tsuru, Evaluating the chemical stability of metal oxides in SO_3 and applications of SiO_2-based membranes to O_2/SO_3 separation, *J. Am. Ceram. Soc.*, 2019, **102**(11), 6946–6956.

This journal is © The Royal Society of Chemistry 2025

Catal. Sci. Technol., 2025, **15**, 2148–2159 | **2159**